INORGANIC CHEMISTRY
FRONTIERS

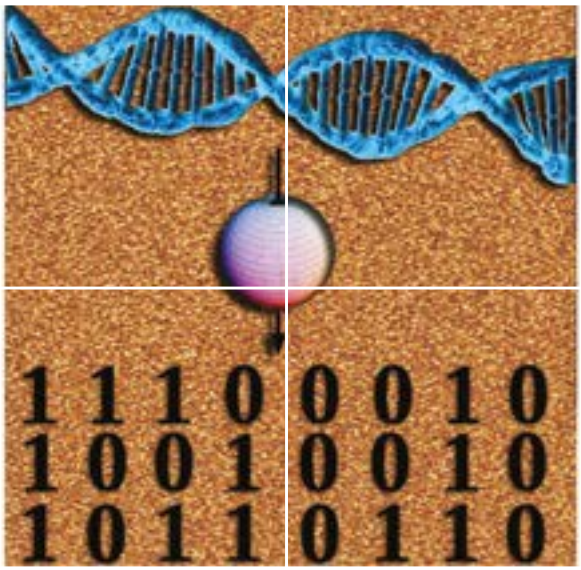


## Accepted Manuscript

This article can be cited before page numbers have been issued, to do this please use: R. Sánchez-de-Armas, N. Cruz Hernández and C. J. Calzado, *Inorg. Chem. Front.*, 2019, DOI: 10.1039/C9QI00129H.

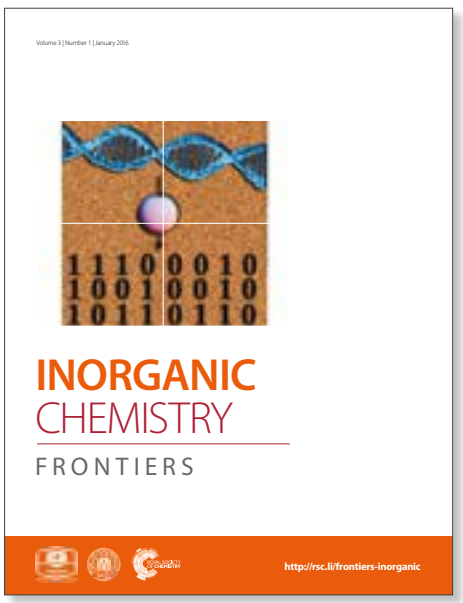


This is an Accepted Manuscript, which has been through the Royal Society of Chemistry peer review process and has been accepted for publication.

Accepted Manuscripts are published online shortly after acceptance, before technical editing, formatting and proof reading. Using this free service, authors can make their results available to the community, in citable form, before we publish the edited article. We will replace this Accepted Manuscript with the edited and formatted Advance Article as soon as it is available.

You can find more information about Accepted Manuscripts in the author guidelines.

Please note that technical editing may introduce minor changes to the text and/or graphics, which may alter content. The journal's standard Terms & Conditions and the ethical guidelines, outlined in our author and reviewer resource centre, still apply. In no event shall the Royal Society of Chemistry be held responsible for any errors or omissions in this Accepted Manuscript or any consequences arising from the use of any information it contains.

View Article Online
DOI: 10.1039/C9QI00129H

# COPPER-NITROXIDE BASED BREATHING CRYSTALS: UNIFIED MECHANISM OF GRADUAL MAGNETOSTRUCTURAL TRANSITION SUPPORTED BY QUANTUM CHEMISTRY CALCULATIONS

Rocío Sánchez-de-Armas,[1] Norge Cruz Hernández[2] and Carmen J. Calzado[1*]

[1]Departamento de Química Física. Universidad de Sevilla. 41012. Spain.

[2]Departamento de Física Aplicada I, Escuela Politécnica Superior, Universidad de Sevilla, 41011, Spain

*corresponding author: calzado@us.es

*Dedicated to Prof. Jean-Paul Malrieu on the occasion of his 80th birthday, for his contributions in the field of molecular magnetism, his permanent curiosity, creativity and generosity.*





**ABSTRACT**

The molecular magnets $Cu(hfac)_2L^R$ based on copper(II) and pyrazolyl-substituted nitronyl nitroxide radicals $L^R$ exhibit thermally and optically-induced magnetostructural transitions, similar to the spin-crossover and light-induced excited spin state trapping phenomena. The mechanism of the gradual change of the magnetic moment in $Cu(hfac)_2L^R$ remains unclear. Herewith, we report a detailed study of this mechanism at molecular level based on DDCI and periodic DFT+U calculations. Three representative members of the $Cu(hfac)_2L^R$ family have been selected, with different substituents (R=Pr, Bu) and solvents (octane, *o*-xylane, without solvent). Our results indicate that the magnetostructural transition can be related to the coexistence of two limit structures, the low temperature (LT) phase with a strong coupling between the Cu(II) and nitronyl nitroxide spins and the high temperature (HT) phase, where the spins are weakly coupled. In this scenario, the gradual change of the magnetic moment with temperature just reflects the thermally weighted ratio of the two limit LT and HT phases. Our finding supports the changes observed on the variable temperature-FTIR spectra of $Cu(hfac)_2L^{Pr}$, manifested by the increase/decrease of certain vibrational bands with temperature and suggest an unified mechanism governing the gradual magnetic anomalies of the $Cu(hfac)_2L^R$ complexes.

## INTRODUCTION

The family of the molecular magnets $Cu(hfac)_2L^R$ based on copper(II) and nitronyl nitroxides (NIT) radicals has been extensively investigated in the last decade for their potential applications as thermal sensors, optical switches, information storage media and other molecular spin devices.[1,2,3,4,5,6,7,8,9,10] They exhibit magnetic anomalies that can be thermally and optically induced, in many aspect similar to classical spin-crossover but of different origin (Figure 1). They present a heterospin polymeric chain structure containing Cu(II) hexafluoroacetylacetonate complexes $Cu(hfac)_2$ with pyrazolyl-substituted nitronyl nitroxides $L^R$ with different substituents (R=Me, Et, Pr, is-Pr, Bu). The polymer chains present two different motifs: (i) a head-to-tail motif resulting in the formation of two-spin Cu(II)-nitroxide clusters, and (ii) a head-to-head motif leading to the formation of an alternating chain of one-spin Cu(II) and three-spin nitroxide-Cu(II)-nitroxide clusters or *spin triads* (Figure 1).

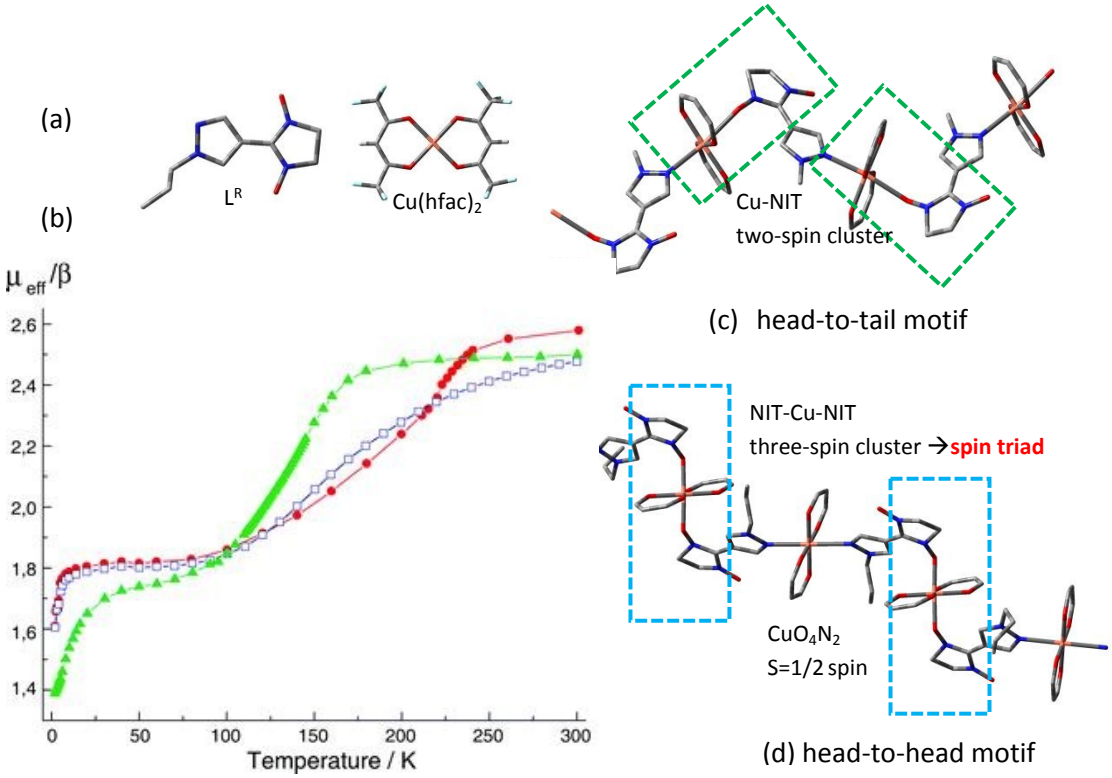


**Figure 1**. (a) Chemical structure of nitronyl nitroxide ($L^R$) and $Cu(hfac)_2$ (b) Temperature dependence of the effective magnetic moment $\mu_{eff}(T)$ of $Cu(hfac)_2L^{Bu}{\cdot}0.5C_8H_{18}$ (**1**) (green triangles), $Cu(hfac)_2L^{Bu}{\cdot}0.5C_8H_{10}$ (**2**) (blue squares) and $Cu(hfac)_2L^{Pr}$ (**3**) (red circles).Reproduced from Ref. [5] with permission from the PCCP Owner Societies. (c) Head-to-tail and (d) head-to-head polymer-chain structure of breathing crystals.

These $Cu(hfac)_2L^R$ complexes undergo reversible structural rearrangements when temperature changes, that modify the interaction between Cu(II) and the nitronyl-nitroxide spins in the spin triads. At low temperatures (LT), nitronyl nitroxides occupy equatorial positions in the coordination shell of Cu(II) ions (Figure 2a). In this coordination, Cu(II) and nitroxide spins are

View Article Online
DOI: 10.1039/C9QI00129H

strongly coupled by an antiferromagnetic interaction (strongly coupled spin state, SS) with a predominant population of the lowest S=1/2 spin state. On increasing the temperature, structural rearrangements occur in $CuO_6$ octahedra that increase the Cu-NIT distance, moving the nitronyl nitroxide ligands to axial positions (Figures 2b and 4). This temperature-dependent switching of the Jahn-Teller elongation axis has been observed in a limited number of copper(II) six-coordinated complexes, as well as a comparable switching related to a pressure-dependent Jahn-Teller rearrangement. Some examples can be found in Ref. 11. Due to these rearrangements, at high temperatures (HT) the spins are weakly coupled (WS, weakly coupled spin state), and the three spin states resulting from their interactions (two doublet and one quartet states) are almost equally populated. As a result, the effective magnetic moment $\mu_{eff}$ increases when the temperature increases (Figure 1b). The change in the magnetic moment can be gradual or abrupt, but in all cases it occurs with a significant change in the unit cell volume. For this reason, these complexes are known as *breathing crystals*.

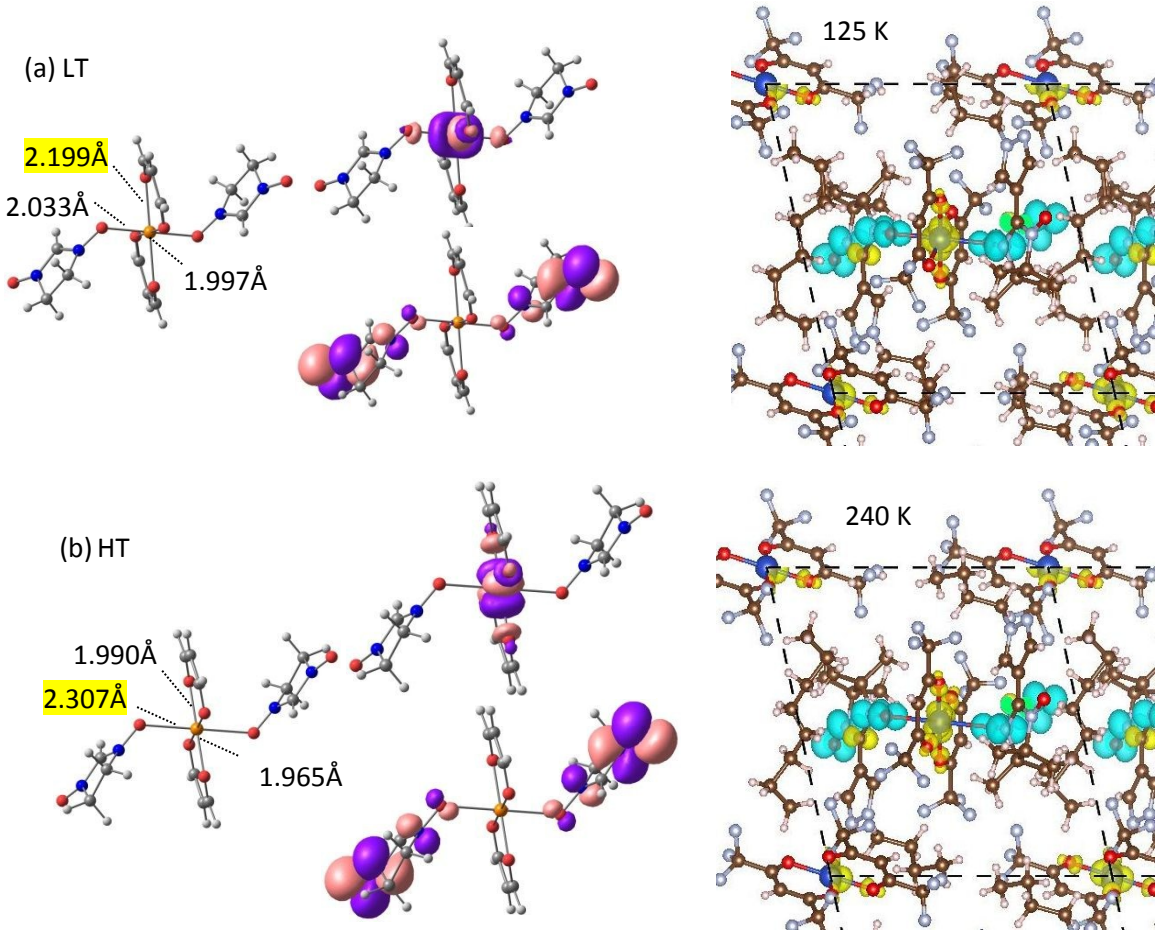


**Figure 2.** (Left-hand column) Spin triad models at low (100 K, top) and high (295 K, bottom) temperature, the distance between the Cu atom and the axial ligand is highlighted in yellow. For LT phase, the NIT groups are in the equatorial positions of the elongated octahedral Cu coordination, while they occupy the axial positions in the HT structure. Orange, red, blue, grey and white balls represent Cu, O, N, C and H atoms, respectively. (Middle column) The Cu $3dx^2$-$y^2$ orbital and the $A_g$ combination of the nitronyl-nitroxide SOMOs, resulting from CASSCF(3/3)

calculation on the quartet state. (Right-hand column) Spin density maps for the AFM solution of $Cu(hfac)_2L^{Bu}\cdot 0.5$ $C_8H_{18}$ (**1**) complex at 125K (top) and 240K (bottom). The unit cell is delimited by dashed lines. View along the *a* axis. Yellow and blue surfaces correspond to positive and negative spin density, respectively.

The $Cu(hfac)_2L^R$ complexes have been widely characterized by X-Ray diffraction (XRD), SQUID magnetometry, electron paramagnetic resonance (EPR) and optical techniques, [2,4,5,7,8,12,13,14,15,16,17] but the mechanism of the gradual transitions at molecular level is not fully understood. Two different interpretations have been proposed to explain the magnetostructural transition[7]:

(i) gradual structural changes in the octahedral $CuO_6$ sites, accompanied by gradual changes in the exchange couplings between Cu(II) and nitroxide spins. This is supported by the X-Ray diffraction data, since they also report gradual changes with temperature (Tables S1-S3 and Figure 4). In this scenario all the spin triads have identical geometry and effective magnetic moment, which are gradually changed when temperature increases, or

(ii) average of the low and high temperature (LT, HT) geometries, that can be in time or in space. Hence the spin triads can be found in one of the two geometries (LT or HT), each one with different magnetic moment. The average can be due to dynamic Jahn-Teller effects that average in time the LT and HT geometries. In this case, fast jumps between the LT and HT geometries occur during the gradual phase transition and then the X-ray, EPR and magnetic susceptibility data exhibit values averaged in time. Alternatively, it is possible to conceive the spatial (or static) average of the LT and HT geometries, i.e., the two phases coexist during the gradual transition in breathing crystals, then the X-ray, SQUID and EPR data correspond to the spatially average of the two structures.

The EPR data of the two phases are clearly different, but the presence of intercluster exchange interactions of about 1-10 $cm^{-1}$ can be sufficient for averaging the EPR lines of the SS and WS states and promote the coalescence in a single signal at intermediate temperatures.[6] Then EPR, although extremely useful in characterizing the breathing crystals, is not helpful to elucidate the leading mechanism at molecular level.

Only recently two independent studies[18,19] have provided relevant indications of the mechanism governing the gradual transitions in *two different members* of the $Cu(hfac)_2L^R$ family. The variable-temperature Fourier transform infrared (VT-FTIR) spectra of $Cu(hfac)_2L^{Pr}$ show vibrational bands with different temperature behaviors, with intensities strongly dependent on the temperature, that can be rationalized assuming the coexistence of the LT and HT phases during the spin transition.[18] A recent theoretical study on the magnetostructural transition of $Cu(hfac)_2L^{Bu}\cdot 0.5$ $C_8H_{18}$ also provide evidences in favor of this mechanism.[19] In this study, the magnetic coupling constants *J* within the spin triads have been evaluated for the X-ray structures reported at different temperatures. The Cu(II)-nitroxide spin

View Article Online
DOI: 10.1039/C9QI00129H





coupling is strongly antiferromagnetic at low temperature and becomes ferromagnetic when temperature increases. The interchain coupling is antiferromagnetic, mediated by the terminal nitroxide groups, and also depends on temperature. The thermal dependence of the effective magnetic moment μ(T) can be reproduced by using the calculated *J* values for each structure to simulate the magnetic susceptibility data. But the μ(T) fitting can be nicely improved by considering the coexistence of two phases in the transition region, which ratio varies with temperature, corresponding to both the weakly coupled and strongly coupled spin states, in agreement with the VT-FTIR study.

The aim of this work is to explore the universality of this mechanism for explaining the *gradual* magnetostructural transitions of the breathing crystal $Cu(hfac)_2L^R$ family, regardless the particular features of each compound, such as the R group or the crystallization solvent. Three illustrative complexes, $Cu(hfac)_2L^{Bu}{\cdot}0.5\ C_8H_{18}$ (**1**), $Cu(hfac)_2L^{Bu}\ {\cdot}0.5\ C_8H_{10}$ (**2**) and $Cu(hfac)_2L^{Pr}$ (**3**) have been considered differing both on the R group substituting the pyrazole moiety (R= butyl or propyl) and the solvent in the interchain voids (solv= octane, o-xylane, without solvent). Our results indicate that the mechanism based on the coexistence of two phases in the transition region, with a thermally modulated weighting ratio, holds for the three analyzed compounds. Moreover, there exists a correlation between the transition temperature and the strength of the Cu-NIT interaction within the spin triads in the LT phase, the stronger the coupling, the higher the critical temperature. This can be considered as an additional indication of the plausibility of this interpretation. Since the examined compounds are representative members of the breathing crystal compounds, our results support the reliability of this mechanism for explaining the *gradual* magnetic anomalies of the $Cu(hfac)_2L^R$ family.

## DESCRIPTION OF THE SYSTEMS

The change in the magnetic moment in the $Cu(hfac)_2L^R$ family can be gradual or abrupt, depending on the R ligand[20] and the crystallization solvent.[21,14] Our study compares the results obtained for three representative compounds, $Cu(hfac)_2L^{Bu}{\cdot}0.5\ C_8H_{18}$ with $C_8H_{18}$=octane (**1**), $Cu(hfac)_2L^{Bu}{\cdot}0.5\ C_8H_{10}$, with $C_8H_{10}$= *ortho*-xylene (**2**) and $Cu(hfac)_2L^{Pr}$ (**3**). Compounds **1** and **2** provide information about the influence of the solvent on the magnetic transition, while the third system could be relevant to discriminate the effect of the external R ligand of the pyrazole moiety. The three considered compounds experience gradual magnetostructural transitions, i.e. the magnetic susceptibility changes smoothly with temperature (Figure 1b), but in a temperature range of different amplitude. Complex $Cu(hfac)_2L^{Bu}{\cdot}0.5\ C_8H_{18}$ (**1**) presents the

View Article Online
DOI: 10.1039/C9QI00129H

narrower temperature range, 75-175 K and a transition temperature of ~130 K.[14] The complex $Cu(hfac)_2L^{Bu}\cdot 0.5\ C_8H_{10}$ (**2**) has a similar behaviour, although the transition region is broader (100-300 K), and the transition temperature is shifted to higher values, $T_c$~190 K. For complex $Cu(hfac)_2L^{Pr}$ (**3**), the transition occurs in the temperature range 100-250 K.[1] Moreover, a structural phase transition occurs at 226 K,[2, 12] the crystal belongs to the $P2_1/c$ space group at low temperature while the space symmetry group is C2/c at T > 226K.



## COMPUTATIONAL DETAILS

*Evaluation of intracluster and interchain interactions by means of DDCI calculations*

The evaluation of the intracluster Cu-nitronyl-nitroxide interaction is carried out on models of the spin triads, while the evaluation of the interchain interactions is based on fragments containing two nitronyl nitroxide groups on neighbour chains. Fragments containing two nitronyl-nitroxide (NIT) groups and the $Cu(hfac)_2$ complex have been selected from the X-ray diffraction data collected at different temperatures. To reduce the computational cost, the external ligands of the spin triad – the pyrazole groups, the -$CH_3$ groups in NIT ligand and the -$CF_3$ groups of hfac – have been replaced by H atoms as in our previous study[19] (Figure 2), with a fixed C-H bond distance of 1.00 Å. Despite the simplifications, the resulting model preserves the geometrical features of the three active centers, in such a way that the effect of the modelling on the amplitude of the *J* couplings is expected to be small if any. The same logic has been employed to build the computational models for the three compounds.

The evaluation of the interchain interactions is based on fragments containing two nitronyl nitroxide groups on neighbour chains. The pyrazole groups have been substituted by H atoms and the coordinates of all the rest of atoms have been extracted from the X-ray data structures of the LT and HT phases (Figure S2). The terminal NO groups are separated by 3.94 Å and 4.09 Å in the case of the structures at 100 K and 295 K of compound **1**, 3.29 Å and 3.47 Å in the case of the structures at 60 K and 295 K of compound **2**. For compound **3**, the NO…ON separation is larger (5.26 Å and 5.29 Å at 50 K and 240 K, respectively), which in combination with the relative orientation of the NO centered $\pi$ orbitals (Figure S2) make difficult this interaction.

The magnetic data for the triad can be interpreted on the basis of the isotropic Heisenberg Hamiltonian:

$$\hat{H} = -2\sum_{ij} J_{ij}\hat{S}_i\hat{S}_j \qquad (1)$$

where $\hat{S}_i$ and $\hat{S}_j$ represents the local spin operator on sites i and j and $J_{ij}$ represents the coupling between them. A spin model with three S=1/2 sites has been considered (Figure 2), with two

types of interactions: *J* corresponds to the interaction between the NIT groups and the Cu center and $J_{NIT}$ is the coupling between the two NIT groups. Notice that term "*site*" in the case of the NIT group in fact refers to a multicentre magnetic site, where the spin density is mainly distributed in the two NO groups (Figure 2). The Heisenberg Hamiltonian on the basis of this model writes as follows:

$$\hat{H} = -2J\left(\hat{S}_{NIT1}\hat{S}_{Cu} + \hat{S}_{NIT2}\hat{S}_{Cu}\right) - 2J_{NIT}\hat{S}_{NIT1}\hat{S}_{NIT2} \qquad (2)$$

The magnetic coupling constants *J* and $J_{NIT}$ can be evaluated from the energy difference of the three eigenvalues of this Hamiltonian, corresponding to two doublet states ($D_1$ and $D_2$) and a quartet state, Q, with energies $E(D_2)= 3J$, $E(D_1)= J + 2J_{NIT}$ and $E(Q)=0$.

In the case of the interchain interaction, the model contains two nitronyl nitroxide groups belonging to neighbour chains, hence, two electron in two site model. The coupling can be determined from the energy difference between the singlet and triplet solutions, E(S)-E(T)= $2J_{chain}$.

In all cases, the energy of the magnetic states is evaluated by means of Difference Dedicated Configuration Interaction (DDCI) calculations.[22, 23] In this approach, all the single and double excitations contributing to the energy difference between the magnetic states are included in the CI expansion. This restriction leaves out the double excitations involving two inactive occupied orbitals and two virtual orbitals and reduces considerably the size of the CI matrix with respect to a complete single and double CI (SDCI) calculation. The procedure requires a common set of molecular orbitals for describing the different states. The MOs of the quartet CASSCF(3/3) state and triplet CASSCF(2/2) states are employed for the evaluation of the intracluster and interchain interactions, respectively. The magnetic orbitals involved in these interactions are shown in Figures 2 and S2.

ANO-RCC type basis functions[24] have been used for all the atoms, with contractions [6s5p3d2f] for Cu, [4s3p2d] for N and O in NIT groups and for C atoms bridging two NO groups, [4s3p] for the rest of C and O, and [2s] for all hydrogen atoms. CASSCF calculations have been performed using the MOLCAS@UU 8.0 program package[25], with the Cholesky decomposition. DDCI calculations have been carried out by means of the CASDI code.[26,27]

*Periodic DFT+U calculations for $Cu(hfac)_2L^{Bu}0.5C_8H_{18}$ at different temperatures*

Additional insight on the electronic structure of these systems can be obtained from periodic density functional theory-based (DFT) calculations. In contrast to those on the spin triad models, the periodic calculations have the advantage of being free of border effects, dealing

View Article Online
DOI: 10.1039/C9QI00129H



with the whole crystal without simplifications and taking explicitly into account the interchain interactions. The three compounds have been previously studied with this methodology but only in the two limit temperatures, LT and HT phases.[28] Here, we extend the study to all the available X-ray structural data of the $Cu(hfac)_2L^{Bu}{\cdot}0.5\ C_8H_{18}$ (**1**) crystal. It belongs to the $P\overline{1}$ space group,[2,5] with a unit cell of 170 atoms. There are four unpaired electrons on the unit cell, three on the spin triad and one on the $CuO_4N_2$ unit (Figure S1). Three different magnetic solutions have been calculated (Figure S1), corresponding to different spin arrangements in the unit cell |NIT-Cu1-NIT…Cu2| with $S_z$=0, 1 and 2:

(i) the AFM solution with Sz=0, $|\uparrow\downarrow\uparrow_K\downarrow|$, where the two NIT groups present an antiferromagnetic coupling with the Cu centre of the triad, and the two Cu centres are coupled ferromagnetically,

(ii) the AFM2 solution $|\uparrow\downarrow\uparrow_K\uparrow|$ with Sz=1 and an antiferromagnetic coupling between the Cu spins, and

(iii) the ferromagnetic solution FM $|\uparrow\uparrow\uparrow_K\uparrow|$ with Sz=2 .

The energies per unit cell of these solutions can be mapped onto the diagonal terms of the Heisenberg Hamiltonian (eq. 1), hence $E_{AFM}= 2J$, $E_{AFM2}= 2J + J'$, $E_{FM}= 0$, where *J*' corresponds to the coupling between the spin triad and the $CuO_4N_2$ unit. *J* and *J*' can then be evaluated from the energy differences between these magnetic solutions.

The DFT calculations have been performed using the Vienna *ab initio* simulation package (VASP) code.[29,30,31,32] The Perdew-Burke-Ernzerhof exchange-correlation functional[33, 34] with the U correction (PBE+U) is employed, with projector-augmented wave (PAW) potentials.[35,36] The +U treatment corrects not only the 3d orbitals on Cu but also the 2p O atoms, as suggested by Morozov *et al*.[37,38] on the related $Cu(hfac)_2L^{Me}$ and $Cu(hfac)_2L^{Et}$ compounds and confirmed by our previous study on breathing crystals.[28] The formulation by Dudarev[39] is used, where the results depends only on the effective U-J values, U and J being the on-site Coulomb (U) and exchange (J) energies, respectively. Effective Hubbard corrections of 9.8 eV for Cu and 5 eV for O have been used, values which have been proven to correctly reproduce the relative stability of the different magnetic solutions, the *J* values and the density of states.[28]

Valence electrons are described using a plane-wave basis set with a cutoff of 500 eV and a Γ-centred grid of k-points is used for integrations in the reciprocal space, where the smallest allowed spacing between k-points is set at 0.2 $Å^{-1}$.[40] Van der Waals interactions were taken into account through the Tkatchenko-Scheffler method.[41] We have considered the reported experimental structures[2] without further refinement at six different temperatures 100 K(=LT),

View Article Online
DOI: 10.1039/C9QI00129H

125, 145, 175, 240 and 295 K (=HT). Electronic relaxation has been performed until the change in the total energy between two consecutive steps is smaller than $10^{-6}$ eV.

## RESULTS AND DISCUSSION

*Evaluation of the magnetic coupling constants at different temperatures*

The $J$ and $J_{NIT}$ values resulting from the DDCI evaluations on the triads at each temperature and $J_{chain}$ for the LT and HT phases are collected in Table 1, together with the $J$ and $J'$ coupling constants resulting from the periodic PBE+U calculations. For all the systems the magnetic interaction between Cu and NIT spins within the triads, $J$, is strongly antiferromagnetic at low temperature and weakly ferromagnetic at high temperature. The changes observed in the calculated $J$ with temperature are in concordance with the changes observed on the effective magnetic moment (Figure 1). The AF-F transition of the DDCI $J$ constants is observed between 125-145 K for **1**, 180-240 K for **2** and 225-232 K for **3**, which is in line with the spin transition temperature reported for these compounds, around 130 K for **1**,[14] ~190 K for **2** and ~200 K for **3**. Our results suggest also a correlation between the value of the magnetic coupling within the triad in the LT phase and the spin transition temperature. In fact, the larger the absolute $J$ value of the LT phase, the higher the transition temperature, following the trend **1** < **2** < **3.** And it is also worth noting that the $J$ value at low temperature mainly correlates with the distance between the Cu ion and the oxygen atom of the NO group. Hence, the strongest $J$ coupling is found for compound **3** with the shortest Cu-$O_{NO}$ distance (Tables S1-S3), and the weakest coupling corresponds to compound **1** with the greatest Cu-$O_{NO}$ separation.

In general, the PBE+U values follow the same trends than the DDCI results, although the PBE+U estimates are larger in absolute value than the DDCI ones. This overestimation is a well-known trend in the case of antiferromagnetic systems, related to the overdelocalization of the electronic density of the magnetic orbitals in GGA-based approaches. [14,37,42,43,44] As a consequence, the AF-F transition at PBE+U level occurs at higher temperatures than those predicted by the DDCI evaluations. For compound **1**, our PBE+U estimate of the $J$ coupling at 145K is still weakly antiferromagnetic, the changes in the PBE+U $J$ values with temperature indicate that the transition should occur at T > 145 K. This is in line with the general overestimation of $J$ found for the PBE+U evaluations. [37,43,45]

The direct interaction between the NIT spins within the triad, $J_{NIT}$, is almost null in all cases. Then this interaction can be safely neglected during the extraction of the interaction parameters at PBE+U level.

View Article Online
DOI: 10.1039/C9QI00129H



**Table 1**. Magnetic coupling constants (in $cm^{-1}$) within the triad, $J$ and $J_{NIT}$, magnetic interaction between the triad and the $CuO_4N_2$ units, $J'$, and interchain couplings, $J_{chain}$, of $Cu(hfac)_2L^{Bu}{\cdot}0.5\ C_8H_{18}$ (**1**), $Cu(hfac)_2L^{Bu}{\cdot}0.5\ C_8H_{10}$ (**2**) and $Cu(hfac)_2L^{Pr}$ (**3**). In bold the values obtained at DDCI level, in italics the values obtained from PBE+U calculations. The $J$ values for the LT and HT phases of compounds **2** and **3** have been included for comparison.[28]

| $Cu(hfac)_2L^{Bu}{\cdot}0.5\ C_8H_{18}$ (**1**) | | | | | | | | |
|---|---|---|---|---|---|---|---|---|
| T/K | 100 | 125 | 145 | 155 | 175 | 240 | 295 | Ref. |
| $J$ | **-145.3** | **-23.5** | **5.1** | **9.0** | **8.3** | **--** | **8.7** | [19] |
| | *-263.5* | *-91.1* | *-2.8* | *--* | *21.3* | *20.9* | *19.2* | *This work* |
| $J_{NIT}$ | **0.2** | **0.3** | **-0.1** | **-0.1** | **0.0** | **--** | **-0.1** | [19] |
| $J'$ | *-3.6* | *0.4* | *-2.0* | *--* | *-0.05* | *-0.8* | *0.06* | *This work* |
| $J_{chain}$ | **-8.3** | | | | | | **-4.4** | [19] |

| $Cu(hfac)_2L^{Bu}{\cdot}0.5\ C_8H_{10}$ (**2**) | | | | | | | |
|---|---|---|---|---|---|---|---|
| T/K | 60 | 100 | 150 | 180 | 240 | 295 | |
| $J$ | **-173.7** | **-173.3** | **-96.2** | **-18.7** | **11.1** | **8.6** | This work |
| | *-322.2* | | | | *24.1* | | [28] |
| $J_{NIT}$ | **0.8** | **0.8** | **1.0** | **0.2** | **-0.4** | **-0.2** | This work |
| $J_{chain}$ | **-0.15** | | | | | **-0.9** | This work |
| | | | | | | *-5.8* | [28] |

| $Cu(hfac)_2L^{Pr}$ (**3**) | | | | | | | | | | |
|---|---|---|---|---|---|---|---|---|---|---|
| T/K | 50 | 115 | 145 | 175 | 195 | 225 | 232 | 240 | 293 | |
| $J$ | **-204.1** | **-171.8** | **-166.2** | **-93.6** | **-46.4** | **-3.4** | **5.0** | **7.6** | **8.1** | This work |
| | *-368.9* | | | | | | | *13.5* | | [28] |
| $J_{NIT}$ | **0.0** | **0.2** | **0.0** | **0.6** | **0.2** | **-0.4** | **-0.1** | **-0.3** | **0.1** | This work |
| $J_{chain}$ | **-0.3** | | | | | | | | **-0.15** | This work |
| | *-2.8* | | | | | | | | | [28] |

The interchain interaction $J_{chain}$ has also been evaluated with both approaches. In all cases, this interaction is weakly AF, although of the same order of magnitude than the Cu-NIT interaction ($J$) at high temperature in the case of compound **1**. Then these two interactions, $J$ and $J_{chain}$ compete at high temperature, dealing to 1D magnetic chains that do not coincide with the polymeric chains in the crystal. This interchain interaction is strong enough to average the EPR signals of HT and LT states[6,19,28] For compounds **2** and **3** the $J_{chain}$ is attenuated with respect to

compound **1**, due to the relative orientation of the π NO-centered magnetic orbitals (Figure S2). For compound **1**, the NIT molecules of two neighbor chains are face-to-face (N-O..O-N torsion angle of 180°), with an optimal π…π overlap. In the case of compound **2**, the torsion angle is also 180°, but one of the NIT molecules is slipped with respect to the other, reducing the π…π overlap, while in compound **3** the π NO orbitals are no more coaxial, since the torsion angle is reduced to 160°. Consequently the antiferromagnetic contribution to the interchain coupling is smaller for compounds **2** and **3** than for **1**.

Regarding the interaction between the triad and the $CuO_4N_2$ spins, a negligible *J'* constant is obtained for compound **1** at all temperatures. This agrees with the description of $CuO_4N_2$ sites provided by EPR as magnetically isolated centers.[5]

*Spin density maps at different temperatures*

The spin density maps of the AFM solution at different temperatures for compound **1** are shown in Figures 2 and S3. They display the change on the relative orientation of the Cu 3d magnetic orbital with respect to the NIT π orbitals when the temperature increases, that can be indeed related to the nature of the interaction between the NIT and Cu spins. At T ≥ 145 K the regions of overlap for the Cu 3d orbital and the NIT π orbitals are almost null, and a ferromagnetic interaction can then be anticipated. In all the cases, the spin density on the terminal nitroxide groups is larger than on the NO directly bonded to the copper ions, in agreement with the picture obtained from polarized neutron diffraction experiments on similar head-to-head nitroxide-Cu-nitroxide systems.[46] This favors the interchain interaction through the terminal nitroxide groups. Also in line with these experiments, the spin density maps show a weak contribution on the C atom bridging the NO groups, with opposite sign than the spin density on them. This feature has also been found in correlated quantum chemistry calculations (post CASSCF) on nitronyl nitroxide-based compounds.[47]

*Simulation of the thermal dependence of the effective magnetic moment*

As mentioned above, different mechanisms have been proposed to explain the magnetostructural transition[7], mainly (i) the transition is due to the gradual structural changes in the octahedral $CuO_6$ sites, accompanied with gradual changes in the exchange couplings between Cu(II) and nitroxide spins, or (ii) the transition is due to the average of the high and low temperature geometries, an average that can occur in time due to fast jumps between LT and HT geometries, or an spatially average due to the coexistence of the two phases. In the

View Article Online
DOI: 10.1039/C9QI00129H

former scenario, each X-Ray data set represents a real structure, and the magnetic susceptibility can be simulated by using the calculated *J* values for each structure. In the second one, the X-Ray data represent just an average of the two limit phases, with different weight depending on the temperature. We analyse hereafter both mechanisms in light of our results.

*Scenario #1: Gradual structural changes*

The molar magnetic susceptibility and effective magnetic moment calculated per $Cu(hfac)_2L^R$ fragment are given by (ignoring diamagnetic contribution):[19]

$$\chi = 0.5\chi_{triad} + 0.5\chi_{mono}$$
$$\mu = \sqrt{3kT\chi / \left(N\mu_B^2\right)} \quad (3)$$

where $\chi_{triad}$ is the molar susceptibility of the NIT-Cu-NIT spin triad in the $CuO_6$ sites and $\chi_{mono}$ corresponds to the molar susceptibility of the Cu ions (S=1/2) in the $CuO_4N_2$ sites:[2,48]

$$\chi_{mono} = \frac{N\mu_B^2 g_{Cu-mono}^2}{3kT} S(S+1)$$
$$\chi_{triad} = \frac{N\mu_B^2}{3kT} \cdot \frac{1.5g_A^2 e^{\frac{-3J}{kT}} + 1.5g_B^2 e^{\frac{-J-2J_{NIT}}{kT}} + 15g_C^2}{2e^{\frac{-3J}{kT}} + 2e^{\frac{-J-2J_{NIT}}{kT}} + 4} + N\alpha \quad (4)$$
$$g_A = \left(4g_{NIT} - g_{Cu}\right)/3,\ g_B = g_{Cu},\ g_C = \left(2g_{NIT} + g_{Cu}\right)/3$$

$g_{Cu}$ and $g_{NIT}$ refer to the g factors of copper and nitroxide within a spin triad and $g_{Cu\text{-}mono}$ to the copper in the one-spin unit. $N\alpha$ corresponds to the temperature-independent paramagnetism (TIP). Finally the interchain (or intercluster) exchange interaction can be also taken into account by means of the mean field approximation, as follows:

$$\mu_{eff}^2 = \mu^2 / \left[1 - \frac{2zJ_{chain}}{3kT} \cdot \frac{\mu^2}{g_{eff}^2}\right] \quad (5)$$

where z is the cluster lattice coordination number (z=2) and $J_{chain}$ is the value of the intercluster coupling constant.

The $\mu_{eff}$ vs T curves using the DDCI *J* and $J_{NIT}$ values are plotted in Figure 3 for the compounds **1-3**. Additionally the fitting for compound **1** obtained with the DFT+U *J* values is also included in Figure 3. In all cases, the gradual change of the effective moment when temperature increases is recovered, with a general agreement with the experimental behaviour. It is worth noting that the magnetic moment fitting curves obtained from the DDCI and DFT+U calculations are quite similar, despite the differences found in the absolute *J* values (see Table 1). At low temperature, once the *J* value is large enough to prevent the occupation of the excited states,

View Article Online
DOI: 10.1039/C9QI00129H

the majority of molecules are in the doublet ground state, and this determines the amplitude of the effective magnetic moment. Then, the absolute value of *J* is not critical for $\mu_{eff}$, once *J* reaches a certain threshold. In the HT phase, the ground state is the quartet, but the excited states are close since the coupling is weak in this phase. At room temperature the thermal energy is large enough to warrant the population of the excited states, and then $\mu_{eff}$ is almost independent of the *J* value.

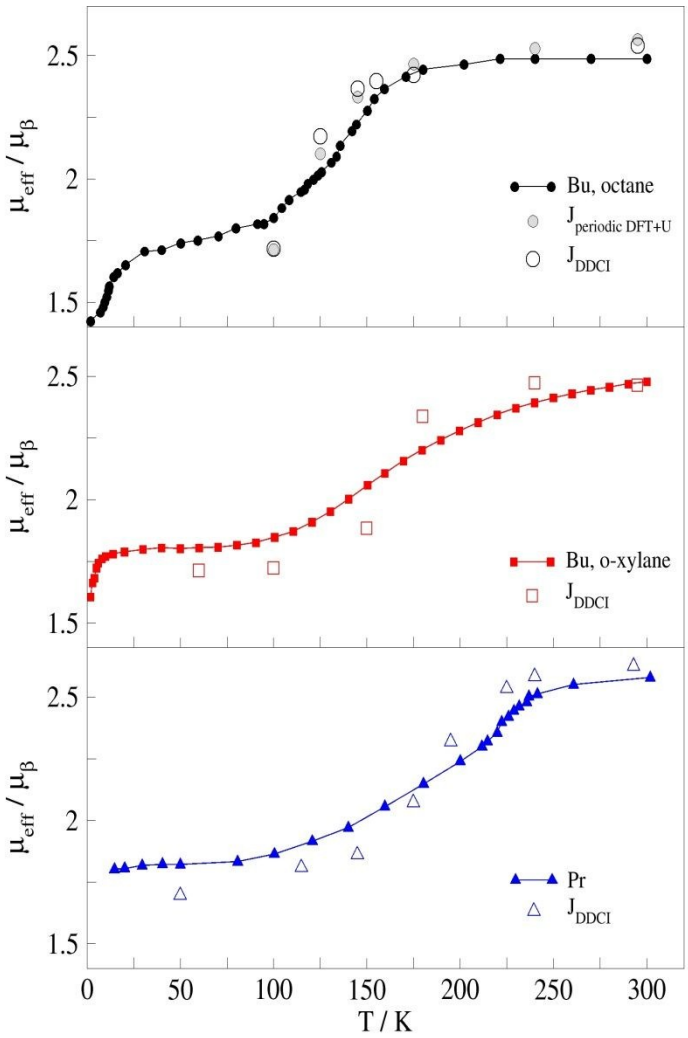


**Figure 3.** Thermal dependence of the effective magnetic moment assuming a gradual change of the magnetic coupling constants due to the gradual change of the structure. Black circle, red square and blue triangle symbols correspond, respectively, to $Cu(hfac)_2L^{Bu}{\cdot}0.5\ C_8H_{18}$ (**1**), $Cu(hfac)_2L^{Bu}{\cdot}0.5\ C_8H_{10}$ (**2**) and $Cu(hfac)_2L^{Pr}$ (**3**) complexes. Closed and open symbols are the experimental and fitted data, respectively. $g_A=g_B=g_C=2$, $g_{Cu\text{-}mono}=g_{eff}=2$ in all cases. $zJ_{chain}$= -16.6 $cm^{-1}$ and TIP=$4{\cdot}10^{-4}$ $cm^3\ mol^{-1}$ for **1**, $zJ_{chain}$ = -2 $cm^{-1}$ and TIP=0 $cm^3\ mol^{-1}$ for **2** and $zJ_{chain}$ = -7 $cm^{-1}$ and TIP=$4.5{\cdot}10^{-4}$ $cm^3\ mol^{-1}$ for **3**. The fitting curve obtained for complex **1** with the DFT+U *J* values is also shown (closed grey circles), with the same fitting parameters than those used for the DDCI results.

View Article Online
DOI: 10.1039/C9QI00129H

The calculated $\mu_{eff}$ vs T curves in Figure 3 show a general agreement with the experimental curves for the three explored compounds, but a close inspection indicates a general overestimation of the slope of this curve in the transition region. Part of this deviation could be assigned to the intrinsic limitations of our computational approach. However, notably different methods as the wavefunction based DDCI calculations on fragments and the plane-wave based periodic DFT+U calculations on the crystal present the same trends. Indeed, the trend is the same for the three compounds, regardless the R group, the presence or not of crystallization solvent and the nature of this solvent. In this context, an alternative analysis of the experimental X-Ray data seems pertinent as shown in the following section.

*Scenario #2: Average of the two limit phases*

In this alternative scenario, we assume that the x-ray data just reflect the average between the two limit phases, which ratio depends on the temperature. Hence, the susceptibility due to the spin triad can be written as:[19,49]

$$\chi_{triad} = w \cdot \chi_{LT} + (1-w) \cdot \chi_{HT} \quad (6)$$

where w and (1-w) are the percentage of LT and HT phases present at each temperature. This weight coefficient can be estimated from the X-Ray data, by considering that in the transition region the Cu-O distances $d_T$ just correspond to the weighted average of the distances in the LT and HT phases:

$$d_T = w \cdot d_{LT} + (1-w) \cdot d_{HT} \quad (7)$$

The weight coefficient w can be obtained using the least-squares method for solving the redundant system of equations for each temperature. The LT and HT phases correspond, respectively to the X-ray structures at 100 K and 295 K for **1**, 60 K (LT) and 295 K (HT) for **2** and 50 K (LT) and 293 K (HT) for **3**. Tables S1-S3 report the Cu−O distances in the spin triad for each X-ray structure, the weight fractions of the LT phase, w, and the weighted $d_T$ Cu-O distances (eq. 7). The comparison of the experimental and weighted Cu-O distances is reported in Figure 4 for compounds **1-3**. The agreement between both sets of data is noticeable for the three compounds, the relative error in the Cu-O distances is small (~0.6-0.8%), 1.5% in the worst case as shown in Table S2 for compound **2**. Then the temperature dependence of the Cu-O distances can be correctly reproduced assuming the coexistence of the two phases on the transition region, which ratio varies with temperature (Figure 4).

View Article Online
DOI: 10.1039/C9QI00129H



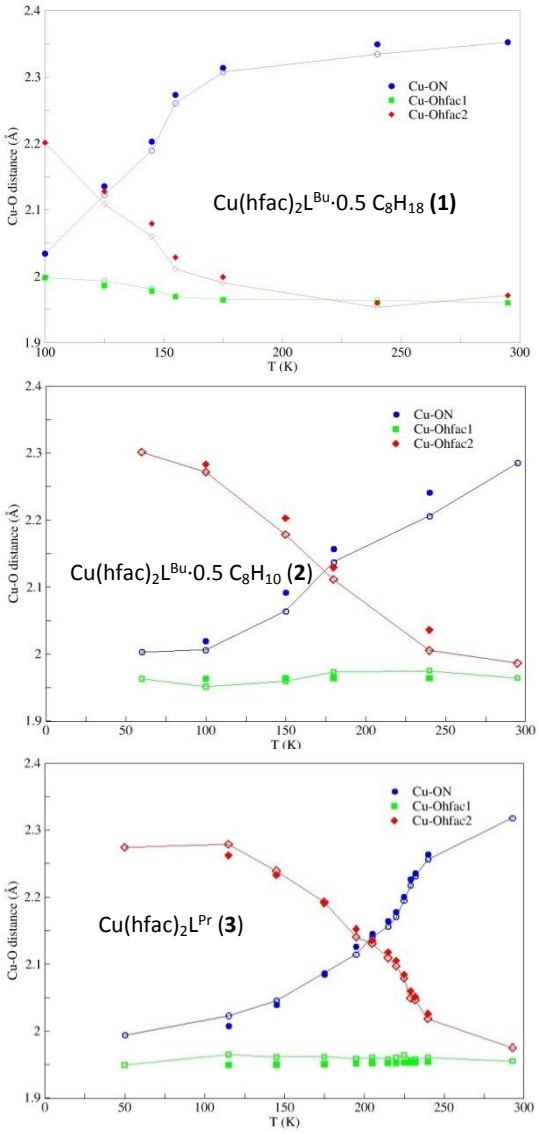


**Figure 4.** Comparison between the reported X-ray Cu−O distances (Å) in the spin triad (open symbols) and those resulting from the average of the LT and HT (filled symbols) for compounds **1** (top), **2** (middle) and **3** (bottom).

Using the same weight factors, the molar susceptibility of the spin triad can be evaluated for each temperature (eq. 6), using the $J$ and $J_{NIT}$ values calculated at DDCI level for the LT and HT phases on each system. The so-resulting μ vs T curves are shown in Figure 5. A nice improvement with respect to the gradual-change scenario is obtained in the three cases, the fitted curves almost match the experimental one on the transition region for the three explored compounds. Then the mechanism previously observed for $Cu(hfac)_2L^{Bu}{\cdot}0.5\ C_8H_{18}$ (the

*proof of concept*)[19] is here confirmed for two other compounds, with different R group and regardless the presence or not of solvent and type of solvent. This suggests that the *gradual* spin transition experienced by many compounds of the $Cu(hfac)_2L^R$ family is governed by a generalized mechanism, a central result of this work.

In this alternative scenario the transition temperature ($T_c$) corresponds to the temperature where the LT phase fraction equals the HT one, i.e. when w=0.5.[50] $T_c$ can be evaluated from the linear fit of the w vs T plot for each compound, interpolating for w=0.5. The so-resulting $T_c$ values are 140.4 K for **1**, 179.5 K for **2** and 209.0 K for **3**, which nicely correlate with the transition temperatures for these compounds,[14] ~130K, ~190K and ~200 K for **1-3**, respectively.

Indeed, this mechanism could explain the correlation found in our calculations between the *J* value at LT and the transition temperature $T_c$. Since at $T_c$ the LT/HT ratio is 1, and the *J* values for the three compounds are almost equal at HT, the differences found for $T_c$ are due to the LT phase, and hence to the amplitude of the dominant interaction. The stronger the Cu-NIT interaction in this phase, the higher the temperature required for populating the excited states responsible for the change of the magnetic moment. These additional evidences support the plausibility of this mechanism based on the thermally-controled average of the LT and HT phases.

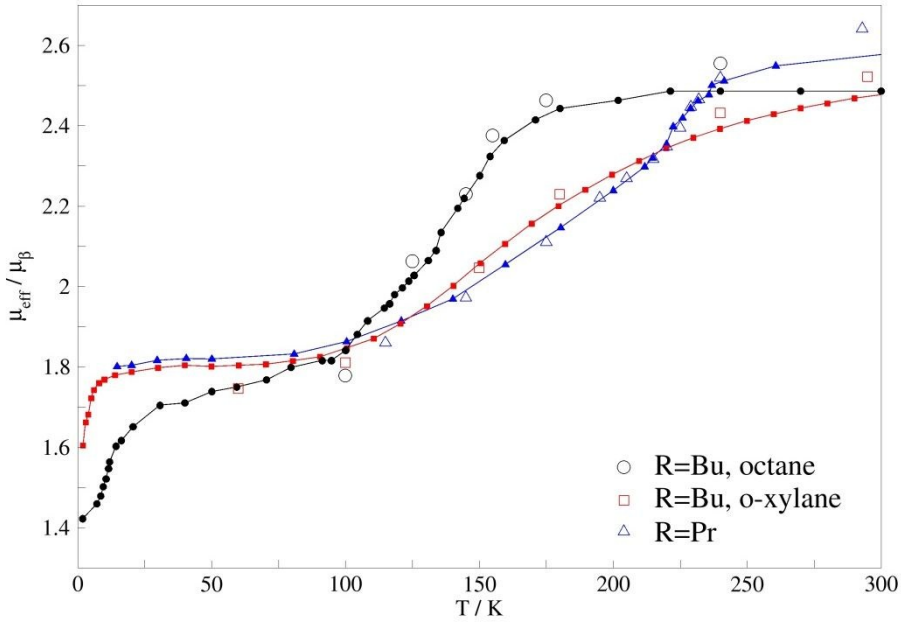


**Figure 5.** Simulated temperature dependence of the magnetic moment assuming the average of the two limit phases, with different weight depending on the temperature. Circle, square and triangle symbols correspond, respectively, to $Cu(hfac)_2L^{Bu}\cdot 0.5C_8H_{18}$ (**1**), $Cu(hfac)_2L^{Bu}\cdot 0.5C_8H_{10}$ (**2**) and $Cu(hfac)_2L^{Pr}$ (**3**). Closed and open symbols are

the experimental and fitted data, respectively. $g_A=g_B=g_C=2$, $g_{Cu\text{-}mono}=g_{eff}=2$ in all cases. $zJ_{chain}$= -4 $cm^{-1}$ and TIP=$3\cdot10^{-4}$ $cm^3$ $mol^{-1}$ for **1**, $zJ_{chain}$= 0 $cm^{-1}$ and TIP=$1\cdot10^{-4}$ $cm^3$ $mol^{-1}$ for **2** and $zJ_{chain}$= = -2 $cm^{-1}$ and TIP=$4\cdot10^{-4}$ $cm^3$ $mol^{-1}$ for **3**.

## CONCLUSIONS

The $Cu(hfac)_2L^R$ molecular magnets have been postulated as promising switching materials exhibiting magnetic anomalies that can be thermally and optically activated. In this work we have explored the mechanism governing the spin transition by means of a combined strategy involving DDCI and DFT+U calculations. The former were carried out on models of the NIT-Cu-NIT spin triads and fragments based on the nitronyl-nitroxide radicals of two neighbor chains to evaluate the intracluster and interchain coupling constants, respectively, at different temperatures. Three representative compounds differing in both the R ligand and the crystallization solvent have been analyzed. Both *J* and $J_{chain}$ present a significant dependence on temperature, in line with the variations observed on the effective magnetic moment. The study is complemented with the evaluations provided by the periodic DFT+U calculations on the whole crystal. These calculations confirm the trends observed by the DDCI calculations on the fragment models, provide also evidences of the isolated magnetic nature of the $CuN_2O_4$ clusters and relevant information about the spin density distribution at different temperatures.

Once the J values have been calculated, the μ vs T curves have been fitted using two dramatically different hypotheses, that is, a gradual change of the *J* values due to the gradual change of the structure, or a gradual change of the magnetic moment due to the thermally weighted average of two limit phases. Our results show that the fitting is nicely improved in the latter scenario.

The reliability of this mechanism is also supported by two additional evidences: (i) the fact that the X-ray data can be reproduced using the same weighting factor w than that used for fitting the μ vs T curves, i.e., the X-ray data just reflect the average between these two limit phases, which ratio depends on the temperature, and (ii) the correlation found between the Cu-NIT *J* coupling at low temperature and the transition critical temperature for the three explored complexes.

Since the selected compounds are representative examples of the diversity of R ligands and crystallization solvent found for the $Cu(hfac)_2L^R$ systems, this study suggests the universality of this mechanism, based on the average of two limit structures, for explaining the gradual transition found for many $Cu(hfac)_2L^R$ breathing crystal compounds, and should be relevant for the potential applications of these switchable molecular compounds.

## CONFLICTS OF INTEREST

There are no conflicts to declare.

View Article Online
DOI: 10.1039/C9QI00129H





**ACKNOWLEDGEMENTS**

The authors acknowledge the financial support provided by the Ministerio de Economía y Competitividad (Spain) and FEDER funds through the projects CTQ2015-69019-P (MINECO/FEDER) and access to the computational facilities of the Red Española de Supercomputación (RES) through project n. QCM-2017-3-0033 and the "Centro de Servicios de Informática y Redes de Comunicaciones" (CSIRC, Universidad de Granada, Spain). R. Sánchez-de-Armas thanks VPPI-US for the financial support.

**SUPPORTING INFORMATION**

Cu-O bond distances within the spin triads for the three considered compounds from X-Ray data, weight fractions of the low temperature phase (w) and Cu−O distances for structures in the transition region estimated as a weighted average of the corresponding distances in the LT and HT structures. Models and magnetic orbitals employed for the evaluation of the interchain interaction, and spin density maps for compound **1** at different temperatures.

**REFERENCES**

1. M. V. Fedin, S. L. Veber, E. G. Bagryanskaya and V. I. Ovcharenko, *Coordination Chemistry Reviews*, 2015, **289-290**, 341-356.
2. M. Fedin, S. Veber, I. Gromov, K. Maryunina, S. Fokin, G. Romanenko, R. Sagdeev, V. Ovcharenko and E. Bagryanskaya, *Inorganic Chemistry*, 2007, **46**, 11405-11415.
3. S. L. Veber, M. V. Fedin, A. I. Potapov, K. Y. Maryunina, G. V. Romanenko, R. Z. Sagdeev, V. I. Ovcharenko, D. Goldfarb and E. G. Bagryanskaya, *Journal of the American Chemical Society*, 2008, **130**, 2444-2445.
4. M. Fedin, V. Ovcharenko, R. Sagdeev, E. Reijerse, W. Lubitz and E. Bagryanskaya, *Angewandte Chemie International Edition*, 2008, **47**, 6897-6899.
5. M. V. Fedin, S. L. Veber, G. V. Romanenko, V. I. Ovcharenko, R. Z. Sagdeev, G. Klihm, E. Reijerse, W. Lubitz and E. G. Bagryanskaya, *Physical Chemistry Chemical Physics*, 2009, **11**, 6654-6663.
6. M. V. Fedin, S. L. Veber, K. Y. Maryunina, G. V. Romanenko, E. A. Suturina, N. P. Gritsan, R. Z. Sagdeev, V. I. Ovcharenko and E. G. Bagryanskaya, *Journal of the American Chemical Society*, 2010, **132**, 13886-13891.
7. S. L. Veber, M. V. Fedin, K. Y. Maryunina, A. Potapov, D. Goldfarb, E. Reijerse, W. Lubitz, R. Z. Sagdeev, V. I. Ovcharenko and E. G. Bagryanskaya, *Inorganic Chemistry*, 2011, **50**, 10204-10212.
8. W. Kaszub, A. Marino, M. Lorenc, E. Collet, E. G. Bagryanskaya, E. V. Tretyakov, V. I. Ovcharenko and M. V. Fedin, *Angewandte Chemie-International Edition*, 2014, **53**, 10636-10640.

9. I. Y. Barskaya, S. L. Veber, S. V. Fokin, E. V. Tretyakov, E. G. Bagryanskaya, V. E. Ovcharenko and M. V. Fedin, *Dalton Transactions*, 2015, **44**, 20883-20888.
10. I. Y. Barskaya, S. L. Veber, E. A. Suturina, P. S. Sherin, K. Y. Maryunina, N. A. Artiukhova, E. V. Tretyakov, R. Z. Sagdeev, V. I. Ovcharenko, N. P. Gritsan and M. V. Fedin, *Dalton Transactions*, 2017, **46**, 13108-13117.
11. M. A. Halcrow, *Chemical Society Reviews*, 2013, **42**, 1784-1795.
12. V. I. Ovcharenko, S. V. Fokin, G. V. Romanenko, Y. G. Shvedenkov, V. N. Ikorskii, E. V. Tretyakov and S. F. Vasilevskii, *Journal of Structural Chemistry*, 2002, **43**, 153-167.
13. V. I. Ovcharenko, K. Y. Maryunina, S. V. Fokin, E. V. Tretyakov, G. V. Romanenko and V. N. Ikorskii, *Russian Chemical Bulletin*, 2004, **53**, 2406-2427.
14. V. I. Ovcharenko, G. V. Romanenko, K. Y. Maryunina, A. S. Bogomyakov and E. V. Gorelik, *Inorganic Chemistry*, 2008, **47**, 9537-9552.
15. M. V. Fedin, S. L. Veber, I. A. Gromov, V. I. Ovcharenko, R. Z. Sagdeev, A. Schweiger and E. G. Bagryanskaya, *Journal of Physical Chemistry A*, 2006, **110**, 2315-2317.
16. M. V. Fedin, S. L. Veber, I. A. Gromov, V. I. Ovcharenko, R. Z. Sagdeev and E. G. Bagryanskaya, *Journal of Physical Chemistry A*, 2007, **111**, 4449-4455.
17. M. V. Fedin, K. Y. Maryunina, R. Z. Sagdeev, V. I. Ovcharenko and E. G. Bagryanskaya, *Inorganic Chemistry*, 2012, **51**, 709-717.
18. S. L. Veber, E. A. Suturina, M. V. Fedin, K. N. Boldyrev, K. Y. Maryunina, R. Z. Sagdeev, V. I. Ovcharenko, N. P. Gritsan and E. G. Bagryanskaya, *Inorganic Chemistry*, 2015, **54**, 3446-3455.
19. J. Jung, B. L. Guennic, M. V. Fedin, V. I. Ovcharenko and C. J. Calzado, *Inorganic Chemistry*, 2015, **54**, 6891-6899.
20. E. V. Tretyakov, S. E. Tolstikov, A. O. Suvorova, A. V. Polushkin, G. V. Romanenko, A. S. Bogomyakov, S. L. Veber, M. V. Fedin, D. V. Stass, E. Reijerse, W. Lubitz, E. M. Zueva and V. I. Ovcharenko, *Inorganic Chemistry*, 2012, **51**, 9385-9394.
21. G. V. Romanenko, K. Y. Maryunina, A. S. Bogomyakov, R. Z. Sagdeev and V. I. Ovcharenko, *Inorganic Chemistry*, 2011, **50**, 6597-6609.
22. J. Miralles, O. Castell, R. Caballol and J.-P. Malrieu, *Chemical Physics*, 1993, **172**, 33-43.
23. J. Miralles, J.-P. Daudey and R. Caballol, *Chemical Physics Letters*, 1992, **198**, 555-562.
24. B. O. Roos, R. Lindh, P. A. Malmqvist, V. Veryazov and P. O. Widmark, *Journal of Physical Chemistry A*, 2005, **109**, 6575-6579.
25. F. Aquilante, L. De Vico, N. Ferre, G. Ghigo, P.-A. Malmqvist, P. Neogrady, T. B. Pedersen, M. Pitonak, M. Reiher, B. O. Roos, L. Serrano-Andres, M. Urban, V. Veryazov and R. Lindh, *Journal of Computational Chemistry*, 2010, **31**, 224-247.
26. D. Maynau, unpublished work.
27. N. Ben Amor and D. Maynau, *Chemical Physics Letters*, 1998, **286**, 211-220.
28. R. Sánchez-de-Armas, N. Cruz Hernández and C. J. Calzado, *Chemistry – A European Journal*, 2018, **24**, 18988-18997.
29. G. Kresse and J. Hafner, *Physical Review B*, 1993, **47**, 558-561.
30. G. Kresse and J. Hafner, *Physical Review B*, 1994, **49**, 14251-14269.
31. G. Kresse, Furthmuller, J., *Computational Materials Science*, 1996, **6**, 15-50.
32. G. Kresse and J. Furthmuller, *Physical Review B*, 1996, **54**, 11169-11186.
33. J. P. Perdew, K. Burke and M. Ernzerhof, *Physical Review Letters*, 1996, **77**, 3865-3868.
34. J. P. Perdew, K. Burke and M. Ernzerhof, *Physical Review Letters*, 1997, **78**, 1396-1396.
35. P. E. Blochl, *Physical Review B*, 1994, **50**, 17953-17979.
36. G. Kresse, Joubert, D., *Physical Review B*, 1999, **59**, 1758-1775.
37. V. A. Morozov, M. V. Petrova and N. N. Lukzen, *AIP Advances*, 2015, **5**, 087161.
38. S. V. Streltsov, M. V. Petrova, V. A. Morozov, G. V. Romanenko, V. I. Anisimov and N. N. Lukzen, *Physical Review B*, 2013, **87**, 024425.
39. S. L. Dudarev, G. A. Botton, S. Y. Savrasov, C. J. Humphreys and A. P. Sutton, *Physical Review B*, 1998, **57**, 1505-1509.

View Article Online
DOI: 10.1039/C9QI00129H

40. H. J. Monkhorst and J. D. Pack, *Physical Review B*, 1976, **13**, 5188-5192.
41. A. Tkatchenko and M. Scheffler, *Physical Review Letters*, 2009, **102**, 073005.
42. J. Cabrero, C. J. Calzado, D. Maynau, R. Caballol and J. P. Malrieu, *Journal of Physical Chemistry A*, 2002, **106**, 8146-8155.
43. R. Sánchez-de-Armas and C. J. Calzado, *The Journal of Physical Chemistry A*, 2018, **122**, 1678-1690.
44. H. J. Kulik, *The Journal of Chemical Physics*, 2015, **142**, 240901.
45. C. J. Calzado, B. Rodríguez-García, J. R. Galán Mascarós and N. C. Hernández, *Inorganic Chemistry*, 2018, **57**, 7077-7089.
46. E. Ressouche, J. X. Boucherle, B. Gillon, P. Rey and J. Schweizer, *Journal of the American Chemical Society*, 1993, **115**, 3610-3617.
47. C. Angeli, C. J. Calzado, C. de Graaf and R. Caballol, *Physical Chemistry Chemical Physics*, 2011, **13**, 14617-14628.
48. C. Benelli, D. Gatteschi, C. Zanchini, J. M. Latour and P. Rey, *Inorganic Chemistry*, 1986, **25**, 4242-4244.
49. E. M. Zueva, E. R. Ryabykh and A. M. Kuznetsov, *Russ Chem Bull* 2009, DOI: https://doi.org/10.1007/s11172-009-0228-7, 1654-1662.
50. R. Boča, *Theoretical Foundations of Molecular Magnetism,*, Elsevier Science 1999, 1999.